Identification and Monitoring of Airborne Volatile Organic Compounds

(BC Clean Air Research Fund)

Final Report

Prepared for

City of Vancouver, Fraser Basin Council, BC Clean Air Research

Prepared by

Dr. Konrad Walus
Department of Electrical and Computer Engineering
The University of British Columbia

Research Team

Prof. Konrad Walus
Prof. Boris Stober
Dr. Suresha K. Mahadeva
Christoph Sielmann
John Berring
Robert Busch
Adriel Lam
Chou Fan
Derek Tsan
Gabriel Man
Tamer Kalla
Tristan Miller

Wednesday, December 5, 2012

Abstract

This project aims to develop technology for continuous monitoring of volatile organic compounds (VOC's) in BC via two primary objectives: the developing of cost-effective, sensitive, and selective continuous VOC sensing technology, and the integration of those sensors into a complete prototype sensing unit. The sensing unit is designed for integration into existing air monitoring equipment and infrastructure in BC. The system is being developed in collaboration with Metro Vancouver and Environment Canada. These agencies are helping to define the proper protocols, interfaces, and sensor specifications. We expect that the final implementation of this new monitoring technology will contribute to a significant cost reduction compared to the current VOC monitoring practices and as a result enable greater deployment of monitoring technology throughout the monitoring network. The sensing technology is based on a low-cost polymeric platform that employs flexural plate wave detection of VOC absorption into polymeric sensing layers. This report details the progress made toward the implementation of this technology and covers the design, fabrication, and characterization of sensing devices and preconcentrator prototypes.

Contents

1 Introduction

Volatile organic compounds (VOCs) are organic chemicals that have a high vapor pressure at ordinary, room-temperature conditions. VOCs are numerous, varied, and ubiquitous. They include both man-made and naturally occurring chemical compounds. Most scents or odors are of VOCs. VOCs have also been found to play an important role in communication between plants. Some VOCs are harmful to human health and contribute to unwanted environmental effects. Anthropogenic VOCs are regulated by law, especially indoors, where concentrations are the highest. Harmful VOCs are typically not acutely toxic, but instead have compounding long-term health effects. Because the concentrations are usually low and the symptoms slow to develop, research into VOCs and their effects is difficult.

As identified by the Environment Canada, VOC's are the major contributes to pollution in the Lower Fraser Valley. Current VOC's measurement systems deployed on field does not provide sufficient data on VOC levels. The availability of a continuous monitoring capability for these chemicals together with the currently available data on wind speed and direction may enable the future identification of VOC emission sources, allowing for more effective enforcement of relevant regulations.

Presently, VOC samples are collected manually in canisters, which are then sent out for chemical analysis at a central location. This approach provides non-continuous data, has an inherent delay in data reporting, and incurs high cost. In this collaborative project with the Metro Vancouver Air Quality Planner and Environment Canada we are developing low-cost and targeted sensing technology for automatic real-time monitoring of VOC's. The sensor units will be specifically designed for integration into the National Air Pollution Surveillance (NAPS) monitoring network and tested at the existing monitoring stations throughout the Lower Mainland.

2 Background

The generation, propagation, and collection of an acoustic wave travelling across a piezoelectric substrate is referred as acoustic sensing. Acoustic sensors have been widely used in numerous fields such as gas analyte measurement, chemical measurement, and biosensing. The type of acoustic wave used by the sensor is, in part, determined by the application and fabrication constraints of the sensor. The majority of substrates used are comprised of stiff materials with high Young's moduli and sufficient thickness to neglect the effects of sensing layer stiffness changes during measurement. Very common piezoelectric substrates include zinc oxide, lithium niobate , and lead zirconate titanate.

Polyvinylidene fluoride (PVDF) is one of the well known piezoelectric polymers however, due to its poor piezoelectric properties and much lower stiffness than the common substrates; it's been less commonly used for acoustic sensing. The use of PVDF combined with flexural plate waves presents an interesting opportunity in acoustic sensing. For the first time our team demonstrate the acoustic sensor employing a PVDF substrate and PEDOT:PSS IDTs, overcoming challenges in poor piezoelectric properties, acoustic wave attenuation, printing on hydrophobic surfaces, and sensitivity to environmental factors such as temperature. The low cost of the sensor materials, data

acquisition technology, and fabrication process, combined with low frequency operation and applications in industrial, commercial, and research sectors, offer the potential for many practical sensing applications.

3 Preparation and Characterization of Piezoelectric PVDF

3.1 Design, Fabrication and Testing of Automated Poling Station

It is necessary to stretch and pole the purchased PVDF film to render this film piezoelectric for usage as our sensor substrate. To enable faster and more consistent stretching and poling, an automated poling station was designed, constructed and tested. The poling station is placed within a controlled temperature chamber and uses an electric motor and data acquisition and control system to stretch the film and apply the necessary high voltages to achieve a consistently stretched and poled film in an automated fashion. Figure 1. and Figure 2. show the automated stretching and poling station. Figure 3 depicts a micrograph of PVDF as purchased that consists of non-piezoelectric α-phase. This material is transformed into piezoelectric β-phase by subjecting it to stretching, followed by electric poling using our automated poling station. The treated PVDF has an oriented fibrillar structure as shown in Figure 4. The amount of phase transformation of PVDF from α- to β-phase is estimated to be 83.3±2.8%.

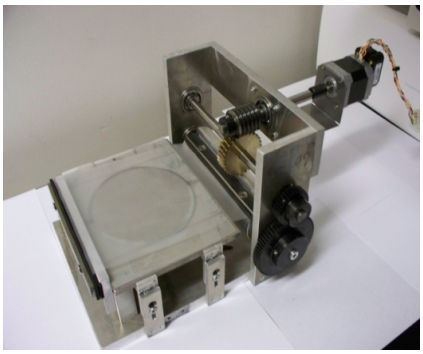

Figure 1: Stretching and poling station without poling dome

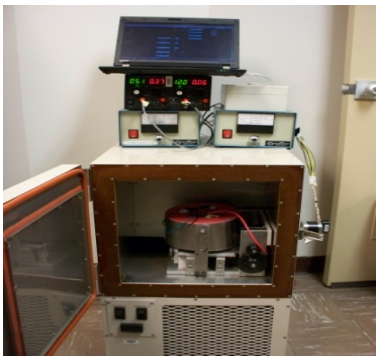

Figure 2: Stretching and poling station with poling dome in an oven

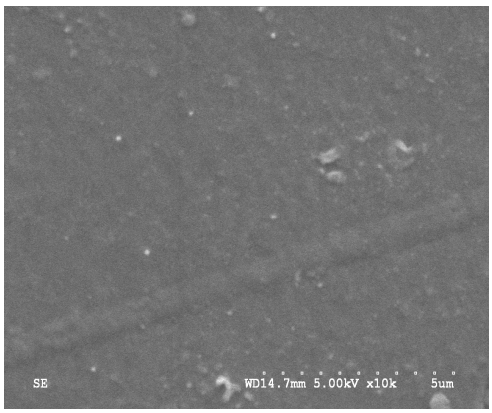

Figure 3: Microphotograph of raw PVDF

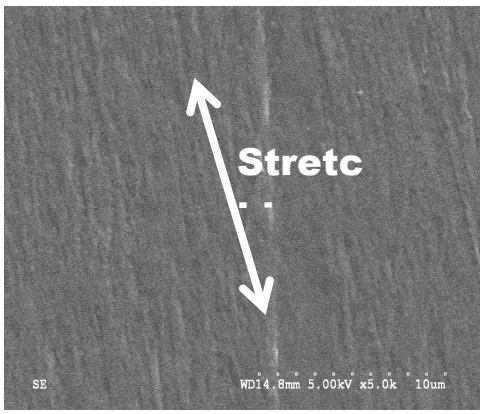

Figure 4: Microphotograph of PVDF after processing.

3.2 Characterization of Different PVDF Types

McMaster Carr has been the default supplier of PVDF for the sensor substrate since the beginning of this project. In an effort to increase the piezoelectric properties of the sensor substrate and to increase the overall sensor performance, the properties of PVDF from a number of different suppliers were investigated. Some of these films were found to produce significantly lower performing sensors and so an investigation was launched into their chemical composition. Mechanical properties, β-phase content, the piezoelectric constant, thermal properties, and crystallinity were compared between samples from McMaster Carr, Proffesional Plastics and Solef. Samples from each supplier were put through our standard PVDF processing procedure. Then the samples were characterized using differential scanning calorimetry (DSC), Fourier transform infrared scpectroscopy (FTIR), dynamic mechanical analysis (DMA) and piezoelectric constant measurement. The results of these tests were used to determine the exact structure of the PVDF obtained from each supplier and to select the best type of polymer for our application. Subsets of the DSC results are discussed here.

A differential scanning calorimeter is a device which determines the amount of energy required to heat a material over a range of temperatures. It is useful as it can provide insight into the thermal properties and crystal structure of a material. The machine heats up the sample past its melting point to 200 ^{o}C and allows it to cool to room temperature. At the melting point, the energy required to change the temperature of the sample increases due to the work required to break the bonds holding the solid together. In the same way heat is released during solidification. This is shown by the respective negative and positive enthalpy peaks in the curve in Fig. 5. The position and shape of these peaks can be used to determine melting point, crystallinity, alpha/beta content, and impurity concentration.

The plot in Fig. 5 shows a set of DSC scans corresponding to a PVDF sample at different steps of the processing procedure. The films (from McMaster Carr) were stretched, contact poled, or corona poled. The plot in Fig. 5 acted as the baseline for all future plots and provided information about the effectiveness of stretching and poling. The relative size and position of the Raw PVDF melting peak and Stretched and Poled

melting peaks suggest that stretching the material will reduce its total crystallinity and the automated/corona poling procedure results in a material with higher beta content.

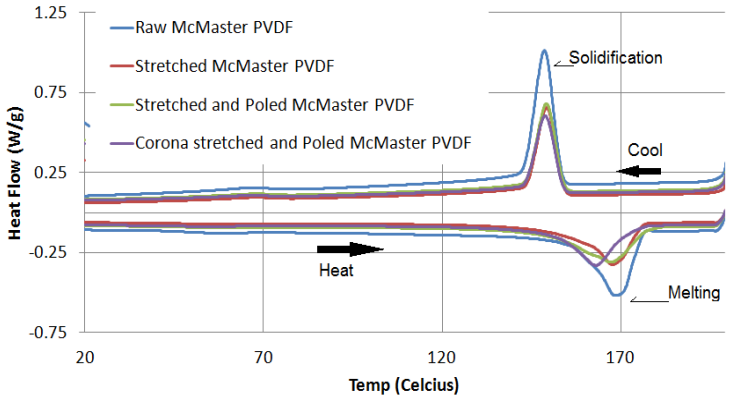

Figure 5: DSC results for PVDF at different stages of processing.

The plot in Fig. 6 shows DSC results for McMaster Carr PVDF, Solef and Professional Plastics PVDF.

One of the key conclusions from that investigation is shown here. The McMaster Carr melting and solidification peaks show the highest peak area. This corresponds with a larger crystalline content in the material. A ferroelectric polymer with a higher crystallinity will have a higher piezoelectric constant as a result. This is believed to be the reason why this material demonstrates better performance.

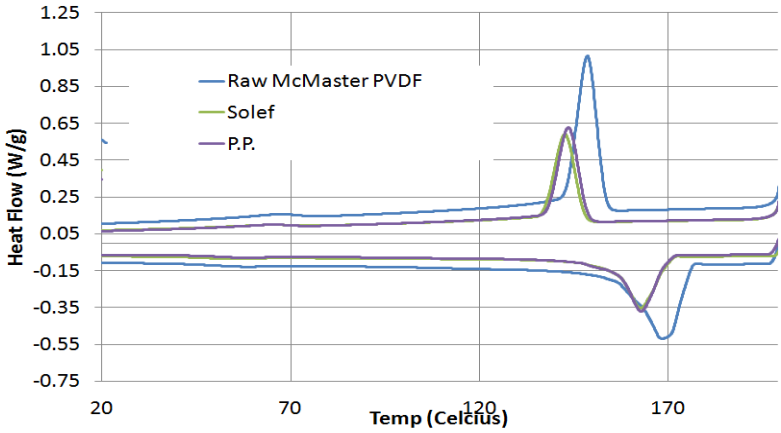

Figure 6: DSC results for PVDF from different suppliers

3.3 Corona poling

There are several parameters in stretching and poling process that affect the piezoelectric property of the resulting polymer. In our corona poling station, ions are generated a three ionization tips at high voltage V_C. These ions are then accelerated toward the substrate that is located on a ground plane. A metallic grid at grid voltage V_G is located a few centimeters above the substrate. As the substrate surface reaches the grid voltage, the additional ions are being collected by the grid, limiting the voltage poling the substrate to the grid voltage. In this study we processed PVDF thin films by varing poling

time (P_T) and grid voltage (V_G), while the rest of the parameters such as the poling voltage (E_P = 15 kV), the stretching ratio (S_R=4) and the temperature (T_P=80˚C) were kept constant. Initially the material consisted predominantly of α-phase; upon processing it successfully transformed to piezoelectric β-phase as evident by XRD analysis shown in Figure 7. β-phase content is determined by comparing the absorbance of the vibration bands of the peaks at 764 and 840 cm^{-1}, which represent α and β-phase, respectively (Figure 8). Assuming that IR absorption follows Lambert-Beer's law and employing following equation

$$\beta = \frac{A_\alpha}{(1.26A_\alpha + A_\beta)},$$

where, A_α and A_β are the structural absorbance's in FT-IR spectrum corresponding to 764 and 840 cm^{-1}, respectively, we were able to calculate the amount of β-phase of the PVDF in Fig. 8 to be 83.3±2.8%.

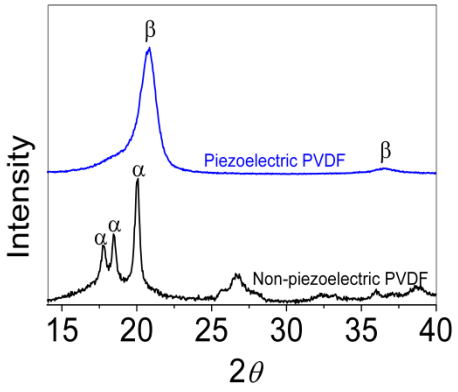

Figure 7: XRD patterns of PVDF

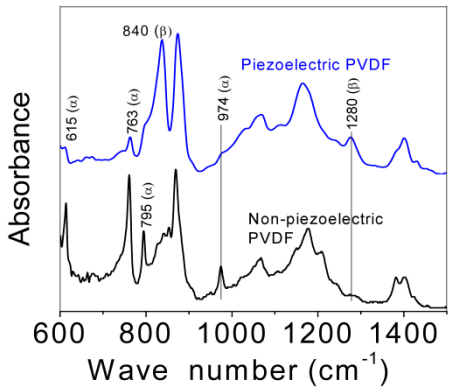

Figure 8: FTIR spectras of PVDF

It is found that above a certain value neither poling time nor grid voltage have any significant influence on the β-phase content of the material. Each PVDF chain has negatively charged fluorine atoms and positively charged hydrogen atoms. These can be arranged on opposing sides of the carbon backbone, through application of a large electric potential during the poling process. This creates aligned dipoles that produce a net polarization. The piezoelectric constant d_{33} increases with poling time due to increased polarization of the material and reaches a maximum of 34.3 pC/N for a poling time of 45 minutes and above. The influence of the grid voltage on the piezoelectric constant d_{33} of PVDF was studied by setting poling time to 45 minutes and the grid voltage is varied from 0 to 6 kV.

3.4 Corona Poled PVDF Sensor Development

As described in previous status reports, two different PVDF processing procedures are used in this project. The first procedure employs manual stretching of the PVDF film in a vice before applying metal electrodes to a small area for contact poling. The second procedure involves the automated stretching system combined with a corona poling process as discussed in the previous section. While contact poling has been used more often throughout the project, it is believed that corona poling will lead to higher

fabrication yields due to its ability to produce larger areas of poled material with fewer dielectric breakdown regions.

A sensor has been successfully fabricated using the corona poling process. It is a 20 µm thick, differential device with an 800 µm acoustic wavelength. Its resonant frequency was measured to be 140 kHz and its output wave amplitude was on par with the average output magnitude of the contact poled devices. Work continues on process optimization as indicated in the previous section and on fabrication of other devices.

4 Fabrication of the VOC's monitoring Sensor

The overall sensor system involves three main components (Figure 8): (i) Preconcentrator (Concentrated gas generator); (ii) Test chamber; and (iii) Measurement system.

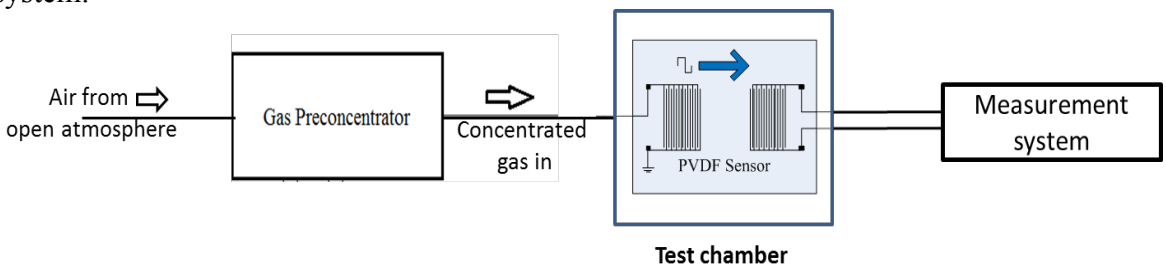

Figure 8. Schematic of the proposed VOC's monitoring sensor system

4.1 Pre-Concentrator

The average ambient concentrations of target analytes ranges from 0.08 to 5 bbp, while the target sensing range of SAW devices is in the ppm range, making it necessary to preconcentrate the sample by a factor of 10^5. This can be done by employing device called "Pre-concentrator". Pre-concentrator typically consists of adsorbent, heating and cooling elements. When the sample air from atmosphere is pumped through an adsorbent for a given sampling time. The VOCs of interest are adsorbed during the sampling process then thermally desorbed and the sensors are exposed to the effluent with a high VOC concentration that is proportional to the inlet concentration.

We chose Carbotrap B as an adsorbent as it is recommended for monitoring C_5-C_{12} compounds. Complete recovery of C_5-C_{10} hydrocarbons from Carbotrap B has been demonstrated by thermal desorption at temperatures up to 320°C.

***Theory*:** We have constructed a model from which the enhancement factor can be estimated using

$$G = \frac{V_{ss} m_A \eta_A}{\frac{m_A}{\rho_A}(1-\chi_A)+V_d},$$

and depends on the desorption efficiency of the adsorbent for the analyte of interest, the sampling volume and the dead volume, where V_{SS} is the safe sampling volume, m_A is the mass of adsorbent, η_A is the desorption efficiency, χ_A is the packing factor and V_d is the dead volume. The safe sampling volume is the maximum volume of sample that can be

passed through the adsorbent before some of the analyte appears in the effluent. There are several different definitions for the safe sampling volume, but it is usually taken to be two thirds of the room temperature 5% breakthrough volume (V_{BT}), which is the volume of sample gas passed through the adsorbent before the concentration of an analyte in the effluent increases to 5% of that in the inlet gas. $V_{SS,}$ and η_A depend on the adsorbent and adsorbate, while the other parameters depend on the design of the preconcentration system.

The maximum safe sampling volume allowed in our design will be dictated by the lowest breakthrough volume of all the analyte/adsorbent pairs. The general trend is for V_{BT} to be proportional to the molecular weight of the analyte. The analytes of concern then are ethylene and 1-Butene on Carbosieve and isoprene, isopentane and 2-Methyl-2-butene on Carbotrap. Using this model we estimate a maximum preconcentration factor of 10^5.

***Experimental*:** A proof-of-concept device was built to demonstrate the pre-concentration process and verify V_{BT} values found in literature. A schematic of the system is shown in Figure 99. V_{BT} of several analytes with Carbotrap were determined using the indirect method whereby a known volume of sample gas carrying a known concentration of analyte is passed through the adsorbent at various elevated temperatures to find the 5% breakthrough volumes. V_{BT} at room temperature is then extrapolated from the high temperature results. The flow rate used in each case was 10 sccm and the typical concentrations were 260 ppm. Figure 10 shows the temperature dependent V_{BT} curves for toluene and xylene. The experimental values were much smaller than values specified by the supplier; these values are compared in Table 1. This is likely due to the low packing density used in our experiments. To improve these results, we are considering a vibration packing system.

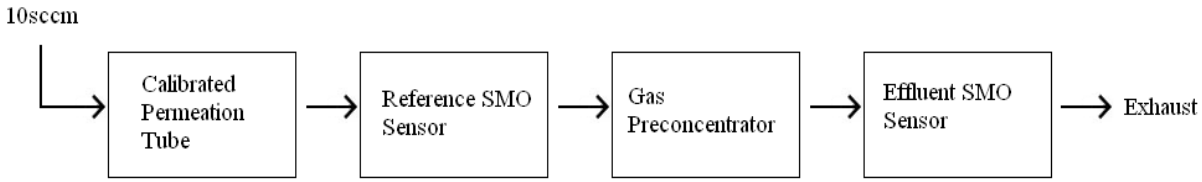

Figure 9: Functional schematic of pre-concentrator test system.

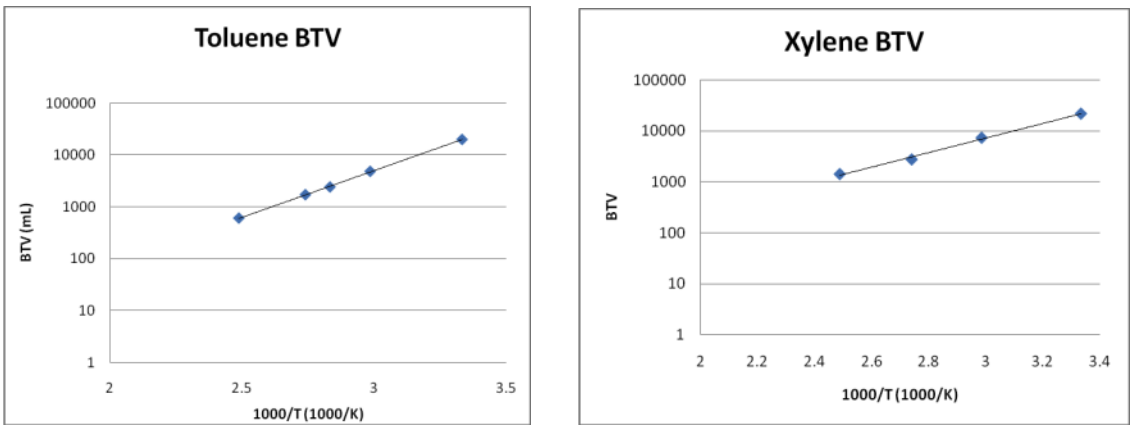

Figure 10: Break through volumes measured as a function of temperature

The enhancement factor for toluene was also experimentally determined. The Carbotrap was exposed to 11 ppm toluene for 40 minutes at a flow rate of 10 sccm. The Carbotrap was then heated to 330°C while still providing 10 sccm of synthetic air to carry the released toluene to the sensor downstream.

Table 1: Breakthrough volumes from experiments and as specified by the manufacturer.

	Experimental V_{BT} (ml/g)	Specified V_{BT} (ml/g)
Toluene	3.98×10^4	6.5×10^5
Xylene	4.34×10^4	4.27×10^7

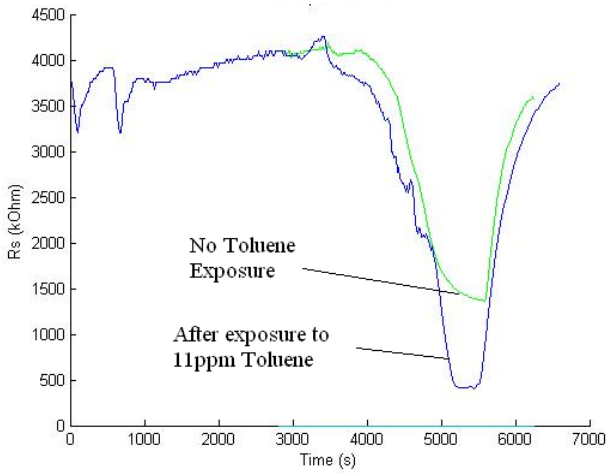

Figure 11: Sensor response over time for Carbotrap with and without toluene.

Synthetic air was used since it does not carry the contaminants found in ambient air that could affect our results. Figure 11 shows the sensor response (resistance) for two experiments. Both included the entire sensing cycle (preconcentrate, heat, sense), one with and one without the toluene gas. There is a clear response of the system to the toluene. Through a large set of experiments we determined a calibration equation for the resistance as a function of temperature and toluene concentration. We used this relationship to determine the enhancement factor from the data shown in Figure 1111. The enhancement factor was found to be 10, which is consistent with this test setup which has significant dead volume and dilution effects associated with the carrier gas. Using this experimental setup, we have verified that Carbotrap is a feasible adsorbent for use in a preconcentrator. It can also be used in future to determine breakthrough volumes of other adsorbent/adsorbate pairs as well as to characterize our SAW sensors.

In order to quantify the performance of the pre-concentrator, a gas sensor is required to measure the output concentration. The plot in Figure 12 shows the calibration curve of our reference gas sensor for toluene. This sensor is not specific to particular VOCs but can serve as a reference for known VOC types.

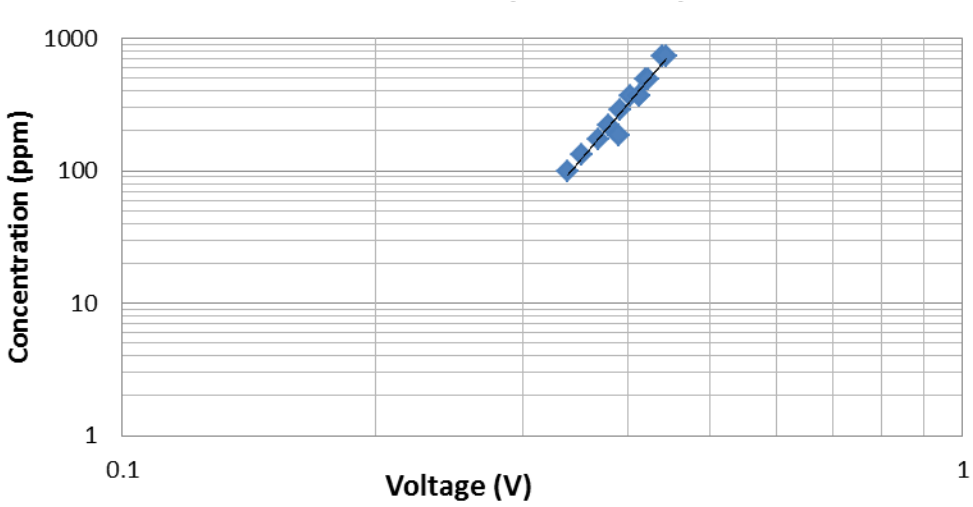

Figure 12: Reference sensor response to toluene concentration.

4.2 Testing/ Sensing chamber

VOC's detecting sensor is made on piezoelectric PVDF substrate, on which an inter digital transducers were printed on one side by employing ink jet printing technique for receiving and transmitting acoustic signals, and sensing layer is deposited on other side of PVDF substrate by drop casting method.

Ink jet printing: An electrode is printed on PVDF substrate using an inkjet nozzle (Microfab Inc.) with an orifice diameter of 40 μm and conductive ink. The ink consists of a mixture of 95 wt% Clevios PH 1000 poly(3,4- ethylenedioxythiophene) poly(styrenesulfonate)(PEDOT:PSS), 5 wt% dimethyl sulfoxide (DMSO) and 0.1 wt% Triton X100 (surfactant). A further detail on fabrication process is found in our published reports listed in section 6 of this report.

***Target Analytes and Analysis Method*:** The degree to which an analyte will adsorb into a polymer can be characterized by the Hansen solubility parameters (HSP) of the analyte-polymer pair. Three relevant bonding parameters are those describing hydrogen bonds, polar bonds, and dispersion bonds (also known as van der Waals forces). These three parameters are often abbreviated to δH, δP, and δD respectively and together form an HSP set that predicts if one material will dissolve in another. Close proximity of an analyte-polymer pair with respect to all 3 HSP indicates a high affinity for adsorption and the polymer could therefore be used as a sensing layer for that analyte. The HSP methodology is an approximation and each analyte/sensing layer pair will need to be characterized experimentally to validate the response. In order to characterise analytes and select appropriate sensing materials, a database of HSP values was acquired. The initial set of volatile organic compound (VOC) analytes targeted for detection as identified by our collaborator at Environment Canada are listed in Table **2**2 together with their HSP values extracted from this database. The VOCs in this set were chosen for their highest measured concentrations in the Fraser Valley by Environment Canada.

Table 2 List of the initial target analytes and their HSP values.

Analyte	**δD ($MPa^{½}$)**	**δP ($MPa^{½}$)**	**δH ($MPa^{½}$)**
toluene	18.0	1.4	2.0
xylene	17.8	1.0	3.1
styrene	18.6	1.0	4.1
α-pinene	15.5	3.0	9.8
isopentane	13.8	0.0	0.0
isoprene	14.7	1.4	4.1
ethylene	15.0	2.0	3.8
1-butene	13.2	1.3	3.9
propylene	13.3	1.6	1.5
2-methyl-2-butene	14.7	2.0	2.9

To visualize the relationship analyte/polymer pairs have using this parametric description, each set can be treated as a coordinate in 3D HSP space. The distance between two substances in this space is a measure of the relative energy difference (RED) between pairs. A low value of RED indicates a high ability for the polymer to adsorb that particular analyte. The target analytes are presented in Hansen Space within Figure 13. Water has also been included as a comparison. Trimethylbenzene has also been included as it is a compound produced during the decomposition of α-pinene, and a compound that we expect will be formed during the high-temperature desorption step required for preconcentration.

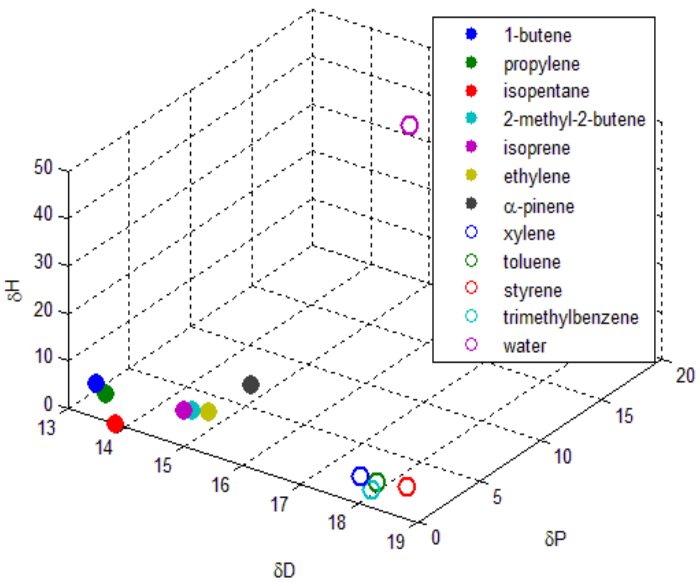

Figure 13: Target analytes and water shown in 3-D HSP space.

As evident from **Figure 13**3, the target analytes we initially identified with Environment Canada essentially form 4 clusters or groups in this domain (5 if we include α-pinene). This grouping is a result of the similarity in the molecular structure of the compounds and hence the nature of the bonding. Since polymers with HSPs matching one particular compound in a group will also be matched to all other compounds in the same group, we expect that our approach will not be able to uniquely identify each analyte individually. Rather, since the groups themselves are quite separated, we will be able to detect all the analytes in a group together and have chosen sensing materials to uniquely identify the 5 groups of analytes. If necessary, we will work with Environment Canada to identify additional groups once the system has been developed.

Selection of Sensing Materials: We selected polymers for each analyte individually such that we minimize the RED values. Analytes that form groups in HSP space will be identified by similar polymers. A list of the selected polymers is given in Verification ***of the HSP Methodology:*** We verified that the HSP methodology is a sensible approach for selecting polymers by performing experiments using our target analytes and the polymer polyisobutylene (PIB). A thin coating of the polymer was deposited onto a Quartz Crystal Micro-balance (QCM), which is essentially a very sensitive mass balance capable of detecting mass changes of less than a micro-gram. A photo of a QCM device used in our experiments is shown in Figure 14. A change in mass is calculated from the measured change in the resonant frequency of the QCM using an impedance analyzer. A decrease in frequency of 1 kHz roughly corresponds to an increase in mass of 90.5 μg.

Table 3. In order to uniquely identify individual groups, we have chosen more polymers than groups, enabling a sort of HSP space triangulation. We will employ methods such as principle component analysis to extract group concentrations from our sensor array measurements.

Verification of the HSP Methodology: We verified that the HSP methodology is a sensible approach for selecting polymers by performing experiments using our target analytes and the polymer polyisobutylene (PIB). A thin coating of the polymer was deposited onto a Quartz Crystal Micro-balance (QCM), which is essentially a very sensitive mass balance capable of detecting mass changes of less than a micro-gram. A photo of a QCM device used in our experiments is shown in Figure 14. A change in mass is calculated from the measured change in the resonant frequency of the QCM using an impedance analyzer. A decrease in frequency of 1 kHz roughly corresponds to an increase in mass of 90.5 μg.

Table 3: Sensing materials for the target analytes in Table 2, HSP parameters of the polymers and RED values for the target-polymer pairs.

Polymer	**δD ($MPa^{½}$)**	**δP ($MPa^{½}$)**	**δH ($MPa^{½}$)**	**Target analyte(s)**	**HSP RED score ($MPa^{½}$)**
2-propenamide	16.9	18.1	19.9	water	1.33
poly(ethyl vinyl ether)	16.0	4.0	12.0	α-pinene	0.19
poly(ethylene vinyl acetate)	18.7	2.3	0.7	trimethylbenzene	0.32
poly(ethylene-co-propylene)	16.6	0.0	5.2	ethylene, isoprene	0.44, 0.46
poly(vinyl acetate)	17.6	2.2	4.0	toluene	0.29
poly(vinyl alcohol)	11.2	12.4	13.0	water, α-pinene	2.54, 1.09
poly(vinyl chloride)	14.9	11.1	3.8	propylene	0.78
poly(vinyl isobutyl ether)	16.0	1.0	8.0	2-methyl-2-butene	0.58
polybutadiene	17.5	2.3	3.4	styrene, xylene	0.39, 0.21
polyethylene	16.9	3.3	4.1	1-butene	0.94
polyisobutylene	14.2	2.5	4.6	toluene, isopentane	0.65, 0.43
polypropylene	18.0	0.0	1.0	xylene	0.29
polystyrene	18.5	4.5	2.9	styrene	0.69

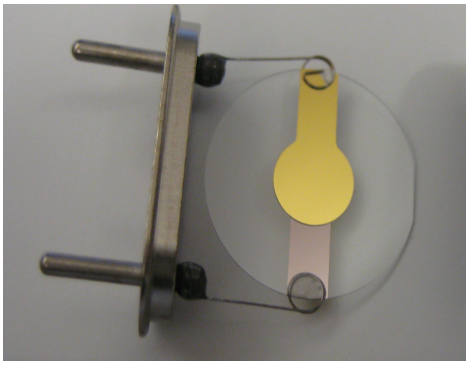

Figure 14: A QCM with a quartz disk that has a diameter of about 14 mm.

Figure 15 shows how the resonant frequency of a bare QCM is reduced through the additional mass of a polymer film (PIB). Exposure to different analytes lowers the resonance frequency confirming that the analytes are being adsorbed by the polymer. We exposed the polymer coated QCM to the saturated head space of the analytes in glass jars that were placed inside a water bath with controlled temperature. Further tests will be conducted in a customized test chamber to better quantify the response and calibrate the fabricated sensors.

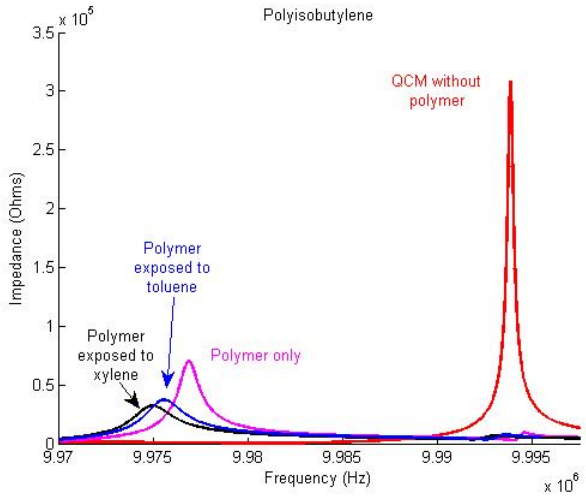

Figure 15: Impedance spectrum of a QCM indicating the resonant frequency shift after applying the polymer and exposure to different analytes.

The ratio of the concentration of analyte absorbed by the polymer to that in the surrounding air is called the partition coefficient, *K*. This quantity can be calculated from theory using the HSP data, as well as determined from our experiments. Table 4 summarizes experimental partition coefficients, K_e, and theoretical partition coefficients for the same pairings. Experimental values shown are averaged over several experiments with the standard deviation shown in parenthesis.

Table 4: Experimental and theoretical partition coefficients.

Polymer / analyte pair	**Mean K_e (± standard deviation)**	**Theoretical *K***
Polyisobutylene / Toluene	5,603 (±524)	4,068

Polyisobutylene / Xylene	9,771 (±119)	15,852

There are several uncertainties associated with both the experimental and theoretical values for the partition coefficients. The theoretical partition coefficients depend not only on the accuracy of the HSP parameters obtained from our database but also on other material properties of the analytes and the polymer such as the molecular weight of the polymer for which we assumed the average value provided by the manufacturer. Additionally, the analyte vapour temperature was difficult to precisely control in our current setup, providing an approximate value for the temperature in the calculation of K and an approximate value for the analyte concentration for the calculation of the experimental K_e. However, the relative difference between the experimental and theoretical values is within tolerances observed by researchers using a different method to measure partition coefficients, and experimental and theoretical values are within the same order of magnitude. While this indicates that HSP parameters provide a route to selecting polymers that are suitable for detecting a particular analyte the exact response of particular polymers to the different analytes will need to be determined with higher accuracy than possible with our current setup. We have recently been awarded a grant that will allow us to construct a customized testing apparatus to increase the repeatability and accuracy of our measurements and enable us to calibrate the fabricated sensors once they are available.

5 Characterization of VOC's/Flexural Plate Wave Sensor

5.1 Device Modeling

During the reporting period, a novel theoretical model of acoustic sensor performance was developed. Previous mathematical descriptions of flexural plate wave (FPW) sensors were determined to be inaccurate as they had been created for common piezoelectric devices based on high stiffness substrates. These models assumed that a frequency shift in the acoustic wave could only be created through mass loading of the sensing layer of the FPW sensor. Given the low stiffness value of the polymer substrate used for the VOC acoustic sensor, this assumption is no longer valid. It was discovered that the resonant frequency of a soft FPW sensor could be shifted by changes in sensing layer stiffness and tension along with mass loading. An analytical model was developed to reflect this and and it was confirmed using experimentation and numerical modeling.

For any flexural plate wave sensor, the phase velocity of the fundamental acoustic wave

$$v_{pa} = \sqrt{\frac{T + \beta^2 D}{M}} \tag{1}$$

may be estimated as a function of tension, T, stiffness, D, mass density, M, and β ($2\pi/\lambda$, where λ is wavelength). Each these terms refer to the combined tension, stiffness and mass density of the substrate and sensing layer. Given a significantly stiffer substrate

than sensing layer, the device sensitivity, or relative change in frequency per unit change in mass

$$S_{FPW} = \frac{-1}{2(M + M_{poly} + \Delta m)} \tag{2}$$

is given by the mass density of the substrate M, the mass density of the polymer sensing layer M_{poly}, and the mass gained through sorption of a gas analyte Δm. Note that the stiffness and tension terms which determine wave velocity and frequency do not contribute here. It is assumed that there will be no variation in D or T. Multiplying S_{fpw} by change in mass will net a fraction which describes the relative change in acoustic wave frequency due to the added material.

For a polymer acoustic sensor, the sensing layer and substrate have Young Moduli which are nearly identical. As such, stiffness and tension variations in the former must be taken into account. The modified sensitivity relationship

$$S_{DM} = -\frac{1}{2(M_{PVDF} + M_{poly,0})} + \frac{3r\beta^2 D_p (d_{PVDF} + d_{poly,0})^2}{2(T + \beta^2 D_p (d_{PVDF} + d_{poly,0})^3)} \tag{3}$$

was derived from equation 1,where d_{pvdf} is substrate thickness and d_{poly0} is initial polymer thickness, and r is the swelling ratio, a term which describes the relative change in polymer volume to mass when exposed to an analyte. When a polymer sensing layer is exposed to a solvent, it will expand as it absorbs the gas or liquid. The expansion will result in an increasing stiffness. Multiplying S_{DM} by change in mass will produce a fraction which describes frequency shift in a mass and stiffness sensitive device.
Note that the two terms have opposite signs. This means that, as mass is added to the sensing layer, frequency will drop due to mass loading but will rise due to an increase in stiffness. The overall shift in resonance is determined by the relative size of each term, and so, mass density, material thickness and polymer swelling ratio.
The performance model was confirmed through finite element analysis and experimentation. The FEA model was developed using the software tool COMSOL Multiphysics using the linear elastic, piezoelectric and electrostatic modules. A screenshot of the resulting 3D simulation is given in Figure 16 (left).

Experimental confirmation was carried out by loading a sensor with successively thicker layers of PVA and measuring the frequency response. Figure 16 (right) shows the experimental results (red points), along with the analytical (green line) and FEA (dashed blue line) predictions. Note that the resonance frequency shift initially falls before rising with PVA thickness. The decreasing frequency is a result of mass loading while the rising frequency is due to increasing stiffness.

Both the analytical model and the FEA model agree well with the measured results. The plot also shows the predicted frequency shift which would be given by the gravimetric, mass only analytical model (dashed green line). In this case, the frequency should have dropped monotonically with increasing PVA thickness.

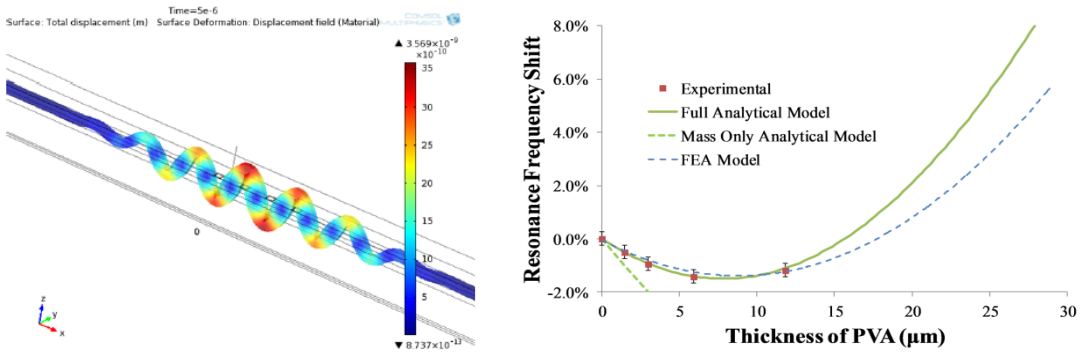

Figure 16: PVDF FPW COMSOL model results (left) and resonant frequency data from experimental, analytical model and FEA model results.

With experimental confirmation, the analytic model was used to explore the design space of the sensor. The two plots in Figure 17 show the expected frequency shift in the sensor as a result of exposure to an identical analyte quantity given different PVDF and sensing layer thicknesses. The left plot shows the response predicted by the mass loading only model while the right plot shows the response predicted by the stiffness and mass loading model.

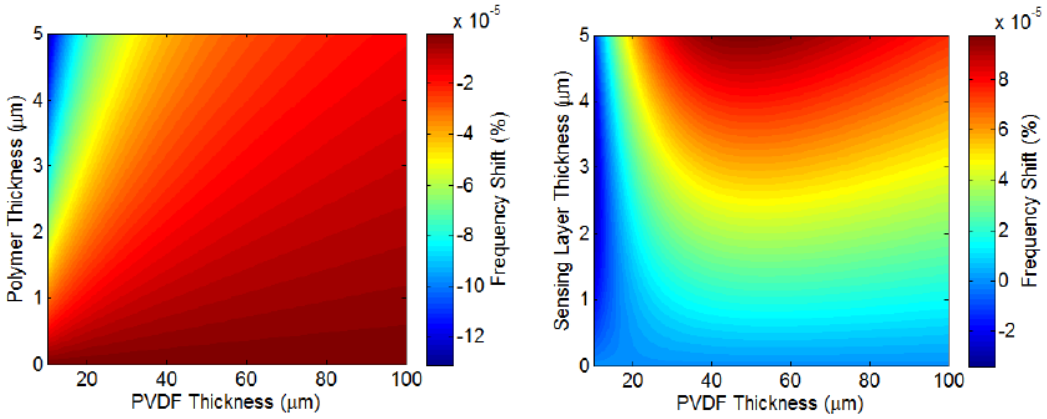

Figure 17: The predicted frequency shift of an 18um thick, 800um wavelength FPW sensor given exposure to a small volume of analyte-calculated using a gravimetric sensing mode (left), and calculated using a gravimetric/stiffness/stress sensing mode (right).

The right hand plot demonstrates that the sensitivity of the acoustic sensor can be adjusted such that it detects primarily mass loading, netting a negative frequency shift, or stiffness change, netting a positive frequency shift. The sensitivity distribution shown here can be further adjusted by changing the inplane tension of the substrate. Applying a higher amount of stress will result in a mass sensitive device while removing all stress will result in a stiffness sensitive device.

These results were combined with further numerical and analytic models to investigate a wide range of proposed sensor design changes. The plots below best sum up the results of this work. They illustrate how changes in various physical, mechanical and electrical parameters will affect the minimum detectable mass change and stiffness change (right)

of the current sensor design (Figure 18). For example, they show that by increasing the thickness of the substrate, the minimum detectable mass and stiffness rise, something which is undesirable. Therefore, the model confirms that the substrate thickness must be reduced to decrease the minimum detectable physical change in the sensing layer.

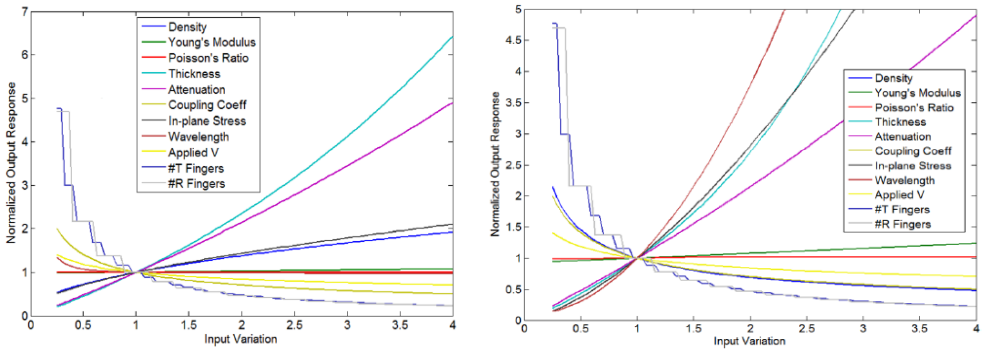

Figure 18: Minimum detectable mass sensitivity (left) and stiffness sensitivity (right) study using an 18 μm thick, 800 μm wavelength differential sensor design as a standard

The results of this study were used to develop optimal design specifications for the next generation polymer FPW sensor, this is discussed further in *Sensor Redesign.*

5.2 PEDOT Backplane

In an effort to improve the signal to noise ratio of the sensor, a conductive backplane was investigated. Prior research had shown that a backplane would significantly increase the field strength beneath the conductive interdigital transducers (IDTs) that form the input or output transducer of the FPW device. As the contraction and expansion of a piezoelectric material is linearly related to the voltage drop across that material, it would be beneficial to concentrate IDT induced electric field in the substrate, rather than the surrounding air. A conductive backplane achieves this by providing a reference voltage region opposite the charged IDTs; in fact, the backplane will assume a potential between the potentials of both electrode pairs of the IDT.

Images from a COMSOL model developed to confirm this are shown in Figure 19. In the top part, one transducer finger is at a high potential while the second one is grounded, and the field in the region is calculated with no ground plane present. The bottom picture shows the same situation with a conductive backplane. Note the higher field intensity within the substrate.

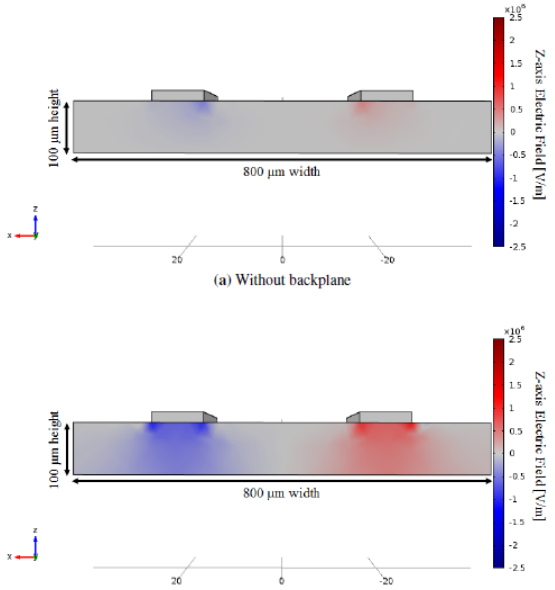

Figure 19: A COMSOL model showing the field intensity around two adjacent tranducer fingers without a conductive backplane (top) and with a conductive backplane (bottom)

A series of sensors were fabricated with a number of different ground plane configurations and materials. The performance of the best device, a sensor coated with three separate backplanes (one for each IDT) is shown in Figure 20. The plot shows the output signal of a sensor without backplane (blue curve) and with a backplane (red curve). Without the backplane, the oscillation amplitude is nearly non-existant. With the backplane, it is increased to 1 Vpp, given x50 output amplification. This addition significantly increased the average signal to noise ratio (SNR) and the quality factor Q of the device, and therefore, the resolution.

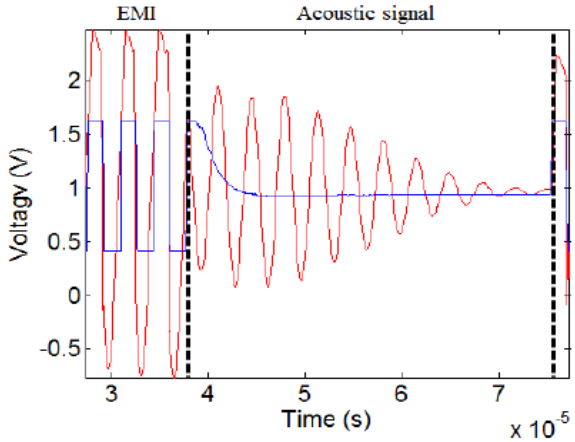

Figure 20: Experimental comparison between an output signal without abackplane (blue) and an output signal with a backplane (red). Thepulses on the left side of the plot show the EMI crosscoupling, withacoustic waves beginning at 38 ms. Saturation of the blue EMI is theresult of a higher gain setting causing clipping of the waveform.

5.3 Humidity Detection

Following the backplane investigation and model development, a series of polyvinyl alcohol coated sensors were fabricated and repeatable, analyte sensing was demonstrated. The sensors were exposed to varying levels of relative humidity (RH) and the resulting frequency, phase and delay shifts were measured as a function of water content in the air. Their performance was then confirmed using the analytical and COMSOL model.

An image of one of these devices is given in Figure 21. It is an 18 µm thick, differential, 800 µm wavelength device based on a stretched and contact poled PVDF substrate. A centre receiving IDT was used to transmit waves to two outer receiving IDTs. On the backside of the device, PVA was dropcast to create 2 to 12 micron thick sensing layers.

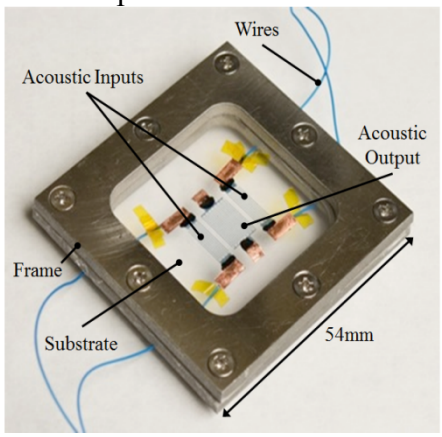

Figure 21: An image of the differential sensor used in this investiagtion

A cross section of the sensor is given in Figure 22 showing the IDTs, sensing layer and substrate. The green layer is a reference polymer, applied to channel B account for environmental factors which may affect the sensor. As polyvinyl acetate does not absorb water, the presence of vapour would not cause a shift in resonant frequency over channel B. If the ambient temperature, relative pressure or substrate tension were to change, on the other hand, this would be reflected in the reference signal. Subtracting this variation from the sensing signal (channel A) would net a less noisy signal.

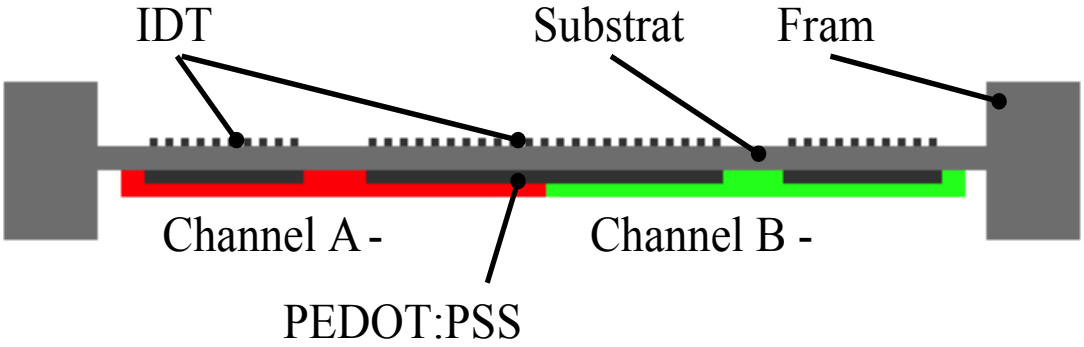

Figure 22: A cross section diagram of the differential sensor used in this investigation

The sensor was exposed to 10% to 60% RH using an Owlstone humidity generator. An image and diagram of the measurement setup is given in Figure 23. The output signal of

the sensor was amplified 50 times before being sent to a 16-bit AD9262 ADC and BF-506F DSP for processing. Using LabView, the frequency, phase, and delay of the output signal was measured and correlated with RH content.

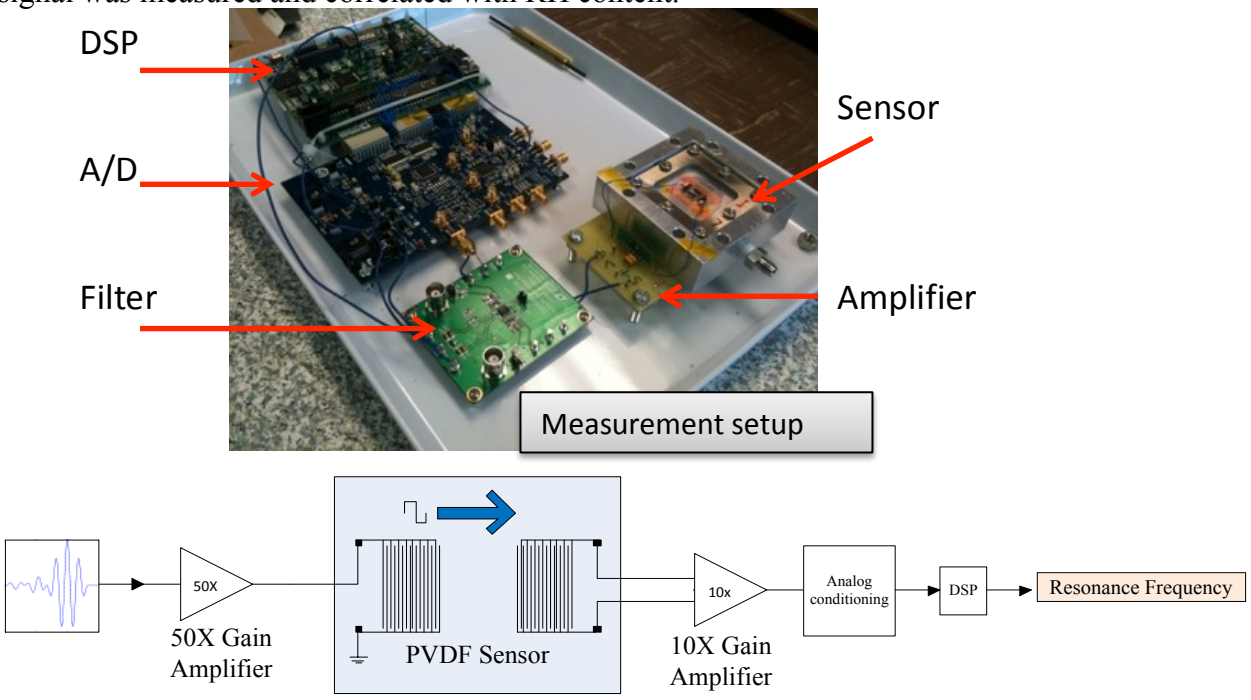

Figure 23: An image (top) and diagram (bottom) of the test setup used in this investigation.

Two plots of sensor response to humidity exposure are given in Figure 24. As water content in the air rises, the resonant frequency of the device falls due to mass loading. With thicker layers of PVA, this trend eventually reverses due to increasing stiffness brought about by PVA swelling. Phase shift, delay, and attenuation were also measured and compared against the numerical and analytical model.

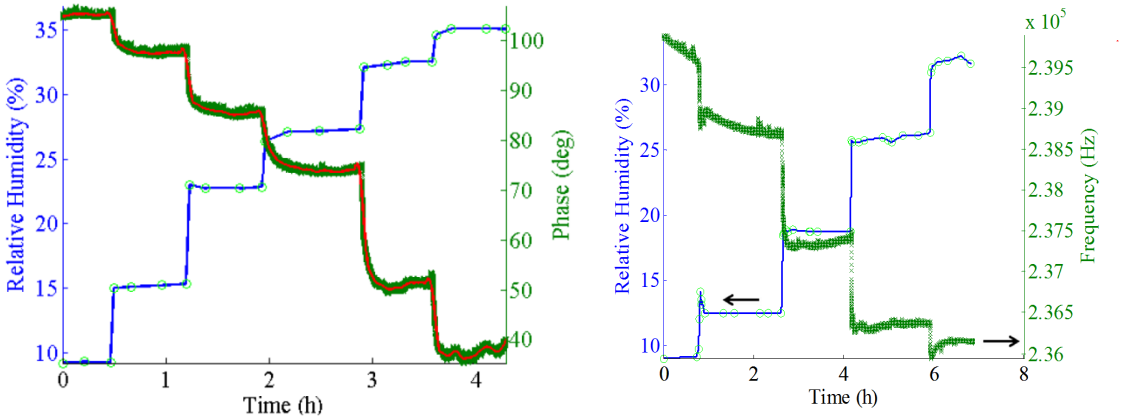

Figure 24: Experimental data of humidity and frequency vs. time with a PVA layer of 6.3 µm. Green points represent the measured frequency response. Red points represent a second order Savitzky-Golay smoothing filter.

These results demonstrate not only a significant improvement in the sensitivity and selectively of the device but also the first successful operation of an all-polymer acoustic wave vapour sensor.

5.4 Polymer-Analyte Characterization

When detecting the presence of a gas, the concentration of the analyte is calculated by measuring a predictable change in sensing layer mechanical properties during exposure. In order to demonstrate humidity sensing and the accuracy of the soft FPW model, the converse was carried out: the sensor was exposed to a known concentration of analyte and the mechanical properties of the sensing layer were deduced.

A 20 µm thick, 800 µm wavelength device was fabricated with a PVA sensing layer. The sensing layer was exposed to varying levels of RH and allowed to soften, swell and gain mass. As shown in Figure 25, the change in stress, stiffness, and mass loading were then calculated as a function of water content in the air. From these results, PVA expansion, Young's Modulus as a function of RH, and partition coefficient were also calculated. This was achieved by fitting the frequency results to equation 1. The physical properties determined with the sensor were compared with values presented in previously carried out research and the results were compared in a recent conference publication.

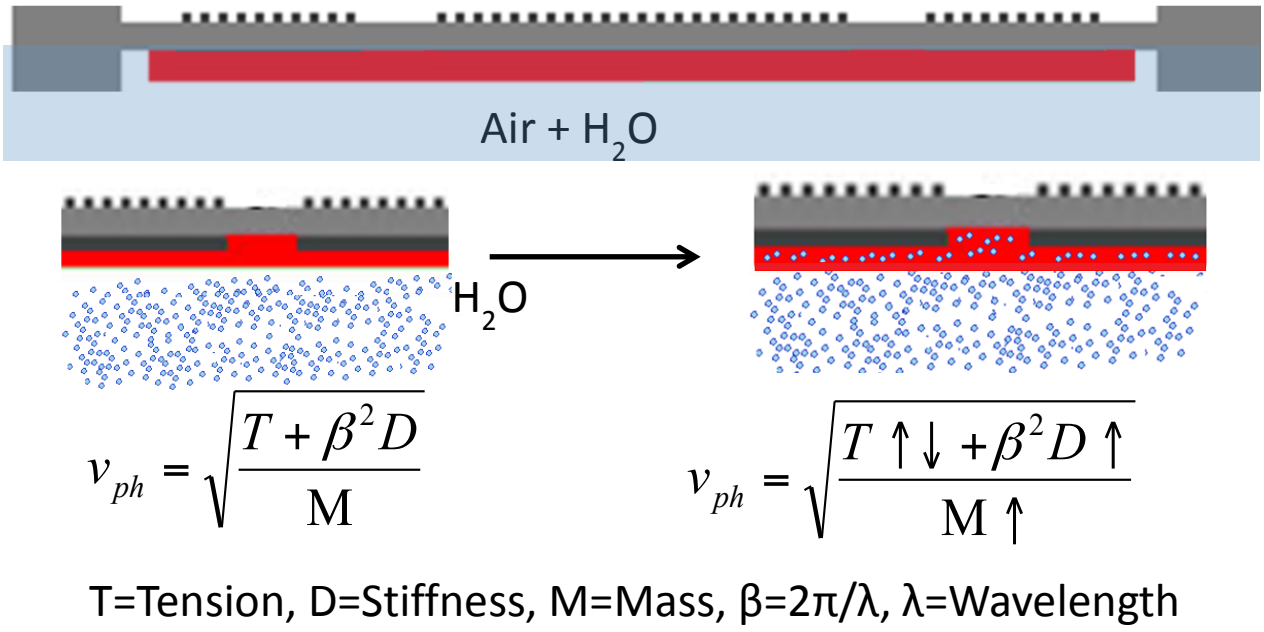

Figure 25: A diagram describing the method for characterizing mass, stiffness and tension in PVA as a function of RH.

Frequency, phase, and signal delay data corresponding to a sensor exposed to 10% to 60% RH were collected for three different PVA thicknesses. The results are given in Figure 20. Here, the points correspond to the resonant frequency of the device for a given RH while the dotted lines correspond to the results of a predictive COMSOL model. The black lines correspond to the results of a least-squares fit of relation 1.

As RH increases, frequency falls, suggesting that mass loading is the primary driver of signal propogation delay. This is consistent with what was previously understood about PVA absorption of water. With the uptake of more fluid the PVA will swell, leading to an increased thickness and become softer, leading to a decrease in Young's modulus. Simultaneously, it will gain mass, leading to a net drop in frequency.

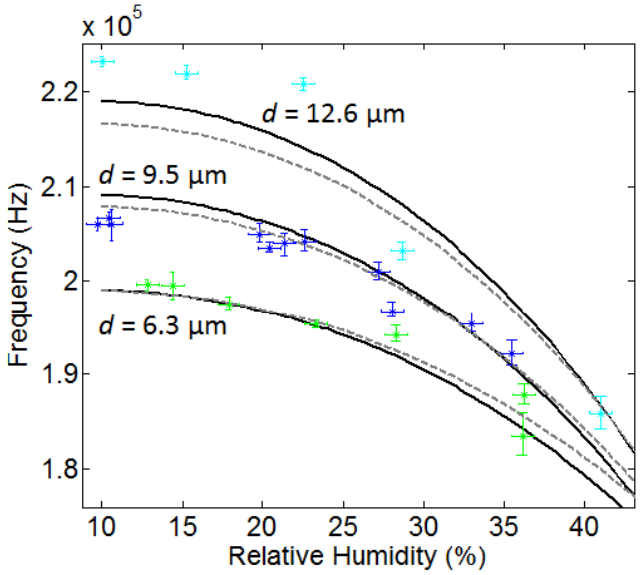

Figure 26: Results from five separate tests involving varying thicknesses of PVA with results from the fitting algorithm shown in black and results from a Comsol Multiphysics simulation shown in dashed grey.

The results from the fit are shown in Figure 27. Here, the percentage change of four properties of interest is presented as a function of relative humidity. The trends agree well with past research.

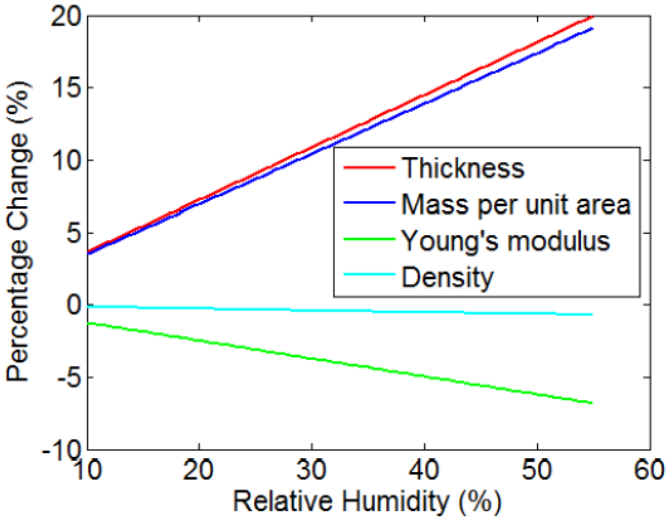

Figure 27: PVA properties as linear functions of humidity based on PVA/PVA fit results.

A comparison of PVA properties measured through the fit and calculated or obtained from previous literature is shown in Table 5. For a full description of the methods used to obtain reference measurements, please see the conference paper "Application of an All-Polymer Flexural Plate Wave Sensor to Polymer/Solvent Material Characterization", attached to this application.

In general, the dry properties of PVA predicted by the fit were on par with those obtained by Experiment/Theory. In comparison, the saturated values of thickness, mass and Young's Modulus were off by up to 19%. This error can be attributed to differences in the type of PVA used in our investigation and PVA experiment as difference in degree of hydrolyzation, density and molecular weight will lead to differences in saturated mass, Young's modulus and thickness.

Table 5. PVA properties from fitting and reference values

PVA Property	From Fit		Experiment/Theory		
	0% RH	52% RH	0% RH	52% RH	Src
Density[kg/m^3]	1266	1259	1269	1230	[1,2]
Young's Modulus [Gpa]	2.67	2.50	2.26	2.10	[3]
Thickness [um/Layer]	3.23	3.82	3.15	3.47	Calc
Mass [g/m/layer]	4.07	4.81	4.00	4.28	Calc
Partition Coefficient	20173	N/A	19700	N/A	Exp

5.5 Reference Layers

A key component of any differential acoustic sensor is the reference layer. This is a material which does not absorb or react with the gas or liquid being detected. It is applied over a second set of IDTs on the substrate such that environmental changes which would affect the sensing channel can be accounted for as indicated above. For example, as the temperature changes, so will the resonant frequency of the device. In order to remove this effect from the output signal, a reference channel is included, and its signalwill shift as a function of temperature but not as a function of analyte concentration.

Finding a suitable polymer to serve this function is not a simple task for certain analytes. When developing the FPW humidity sensor, a series of reference polymers were

[1] J. Krzeminski and H. Molisak-tolwinska, "The Structure of Water- Swollen Poly(Vinyl Alcohol) and the Swelling Mechanism," Journal of Macromolecular Science: Part A - Chemistry, vol. 28, no. 3–4, pp. 413–429, 1991.

[2] Sigma-Aldrich, "Poly(vinyl alcohol) #363081 MSDS", Internet:http://www.sigma-aldrich.com, May 2012 [July 2012].

[3] M. V. Konidari, K. G. Papadokostaki, and M. Sanopoulou, "Moistureinduced effects on the tensile mechanical properties and glass-transition temperature of poly(vinyl alcohol) films," Journal of Applied Polymer Science, vol. 120, no. 6, pp. 3381–3386, 2011.

investigated. These materials were chosen based on their low water solubility, however, very few were sufficiently unresponsive to the presence of humidity.

The reference layers were tested by drop casting layers of each polymer ranging from 2 µm to 15 µm on the back of a sensor. The sensor was then exposed to varying levels of RH and the response was measured over both channels. A plot showing the phase shift of a set of polymers investigated is shown in Figure 28. A perfect reference material would show no frequency or phase shift as a function of RH. As illustrated in Figure 28, polystyrene (PS), polyvinylidene fluoride (PVDF), and parylene all show significant frequency shifts, despite having no ability to absorb water.

This phenomenon is likely as a result of water adsorption. While the materials cannot be dissolved by water, they can physically adsorb water. If the polymers are sufficiently porous, it is thought that enough water could be adsorbed to lead to a mass loading driven frequency shift.

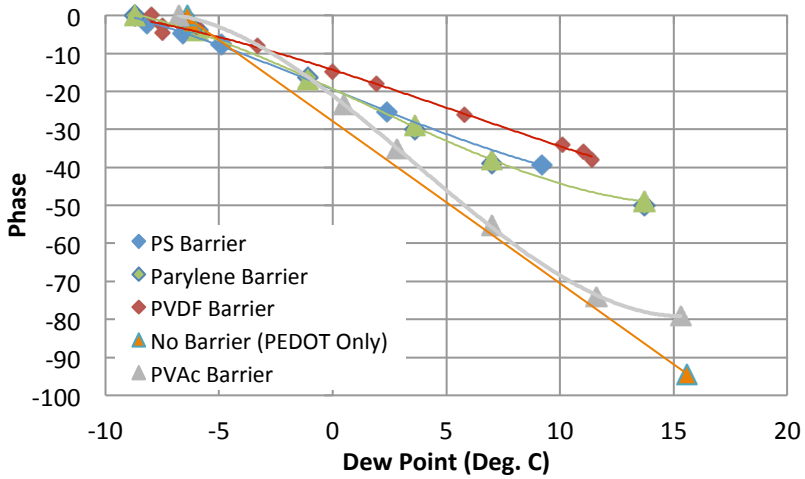

Figure 28: A plot showing phase response of a sensor coated with various reference polymers and exposed to different levels of RH.

This work led to a better understanding of available reference layers and resulted in PVDF being chosen as the default analyte barrier for future tests.

5.6 Toluene Sensing

Following the successful detection of humidity and confirmation of the soft FPW sensor model, an investigation into toluene sensing was initiated. A series of 18 µm thick, differential, 800 µm wavelength sensors were fabricate with 6 µm polyvinyl acetate sensing layer and a polyvinylidene flouride reference layer. These sensors were exposed to varying concentrations of toluene vapor and the frequency shift on the sensing channel (PVAc) was measured. With our initial results, we have demonstrated the detection of toluene and are currently in the process of analyzing and compiling the report on this part.

5.7 Future Steps: Sensor Design Improvements

The sensitivity, quality factor and SNR of the FPW sensor have improved significantly over the reporting period. This has primarily been due to extensive modeling work undertaken at the end of 2011 and beginning of 2012. Newly developed analytic and numerical models have allowed the accurate prediction of device performance prior to fabrication. This has lead to a set of design and fabrication goals which can be directly linked to performance.

The table below shows the key characteristics of our current sensor design (left column) and a future design (right column). The sensitivity of the latter design will meet and exceed that which is required for a VOC sensor working in tandem with a preconcentrator. It was created to act as a waypoint in sensor development, neither representing the final sensor configuration, nor that which meets minimum required sensitivity goals. Instead, it is the highest sensitivity device which could be fabricated using currently available materials.

Research is now carried out with this goal in mind. However, achieving the future design will be no trivial task. The primary barrier to overcome is associated with the thickness of the substrate. In order to achieve the sensitivities listed below, a 500nm thick substrate is required. Fabricating a polymer piezoelectric film of this dimension will require the development of entirely new manufacturing and processing techniques.

Beyond this, further sensitivity improvement can be achieved if substrate tension, attenuation and Young's modulus are reduced while electromechanical coupling coefficient, piezoelectric coefficient and IDT conductivity are increased. These modifications will also be investigated in the coming months.

Table 6. Current sensor characteristic and those of a future design.

Criteria	Current 18 μm Design	Future 0.5 μm Design
Volume	3.75 cm^3	1.65 cm^3
Operating Frequency	215 kHz	9.5 kHz
Signal Strength	9.68 μW	100 μW
Quality Factor	13.3	308
Mass Sensitivity	-156 cm^2/g	-4682 cm^2/g
Stiffness Sensitivity	32570 /Nm	5×10^6 /Nm
Δm_{min}	4.80 $\mu g/cm^2$	4.1 ng/cm^2
ΔD_{min}	2.30×10^{-8} Nm	3.85×10^{-18} Nm

6. Reference for further reading

1. "Inkjet printed all-polymer flexural plate wave sensors"
http://ieeexplore.ieee.org/xpl/articleDetails.jsp?arnumber=6170181

2. "Implications of a Low Stiffness Substrate in Lamb Wave Gas Sensing Applications"
http://sensors2012.epapers.org/ESR/paper_details.php?paper_id=1307

3. "Application of an All-Polymer Flexural Plate Wave Sensor to Polymer/Solvent Material Characterization"
http://sensors2012.epapers.org/ESR/paper_details.php?paper_id=1969